Available online at www.sciencedirect.com
ScienceDirect
Journal of Molecular Catalysis A: Chemical 285 (2008) 29–35
JOURNAL OF MOLECULAR CATALYSIS A: CHEMICAL
www.elsevier.com/locate/molcata

Selective hydrogenation of *p*-chloronitrobenzene over Ni–P–B amorphous catalyst and synergistic promoting effects of B and P

Hui Li, Qingfei Zhao, Hexing Li *

Department of Chemistry, Shanghai Normal University, Shanghai 200234, PR China

Received 28 July 2007; received in revised form 12 January 2008; accepted 15 January 2008
Available online 20 January 2008

Abstract

Ni–P–B amorphous alloy catalyst was prepared by chemical reduction of Ni^{2+} with KBH_4 and NaH_2PO_2 as co-reducing agents. During liquid-phase hydrogenation of *p*-chloronitrobenzene (*p*-CNB), Ni–P–B exhibited higher activity and better selectivity to *p*-chloroaniline (*p*-CAN) than either Ni–B or Ni–P, obviously owing to the synergistic promoting effects of both the P and the B co-alloying with the metallic Ni. The P promoted hydrogenation activity via enhancing the intrinsic activity (R_H^S) since the Ni active sites alloying with P became more highly unsaturated, which could adsorb hydrogen more strongly, taking into account that *p*-CNB hydrogenation was first-order with respect to hydrogen. The B promoted hydrogenation activity via enhancing the dispersion degree of Ni active sites. The higher selectivity to *p*-CAN could be attributed to the inhibition of hydrodehalogenation since the metallic Ni alloying with P could adsorb the nitro group preferentially against the chlorine atom in *p*-CNB. Meanwhile, the presence of the alloying B could further enhance the adsorption strength for nitro group via side-bonding and also protected Ni active sites from poisoning by the amine resulting from *p*-CNB hydrogenation.

Keywords: Ni–P–B amorphous alloy catalyst; Synergistic promoting effects; Hydrogenation; *p*-Chloronitrobenzene; *p*-Chloroaniline

1. Introduction

Haloanilines are widely used in manufacturing dyes, drugs, herbicides, pesticides, and other fine chemicals. In comparison with traditional synthesis routes [1,2], the selective hydrogenation of halonitroaromatics to corresponding haloanilines is superior in saving resources, reducing waste disposal and protecting the environment [3,4]. However, it is a challenging task to accomplish selective hydrogenation of the nitro group since the dehalogenation usually occurs [5–7]. To achieve high selectivity towards haloanilines, great attempts have been made to develop new and powerful catalysts [8–21]. Most studies are focused on precious metal catalysts, such as Pd, Pt, Rh, and Ir-based catalysts. However, the high cost seems problematic in the industrial application. Recently, amorphous alloys have been widely used in hydrogenation reactions owing to their higher activity, better selectivity, and stronger sulfur resistance relative to their crystalline counterparts, among which Ni–P and Ni–B amorphous alloys are perhaps the most thoroughly studied [22–25]. Generally, Ni–B amorphous alloys are active while Ni–P amorphous alloys are selective in hydrogenations [26,27]. By chemical reduction of nickel acetate with sodium hypophosphite and sodium borohydride, Wang et al. prepared Ni–P–B catalyst, which had been demonstrated to be a good catalyst for *p*-chloronitrobenzene (*p*-CNB) hydrogenation [28]. However, no systematical studies on the synergistic promoting effects of both the alloying B and P on the catalytic performances have been reported so far. In this paper, Ni–P–B amorphous alloy catalyst was prepared via co-reducing Ni^{2+} with mixed KBH_4 and NaH_2PO_2 and its catalytic behaviors were examined and compared with Ni–P and Ni–B amorphous alloy catalysts during liquid-phase *p*-CNB hydrogenation to *p*-chloroaniline (*p*-CAN). Based on various characterizations, the synergistic promoting effects of the B and P co-alloying with the metallic Ni were discussed briefly.

2. Experimental

2.1. Catalyst preparation

Ni–P–B sample was prepared by chemical reduction according to the following procedure. An aqueous solution containing

* Corresponding author. Tel.: +86 21 64322272.
E-mail address: HeXing-Li@shnu.edu.cn (H. Li).

1381-1169/$ – see front matter © 2008 Elsevier B.V. All rights reserved.
doi:10.1016/j.molcata.2008.01.025

2.0 M KBH_4 was added dropwise into an aqueous solution containing 0.31 M $NiCl_2$ and 1.25 M NaH_2PO_2 at 303 K. The system was kept for vigorous stirring until no gas released. The resulting black solid was washed free from Cl^-, K^+ and Na^+ ions with H_2O, followed by washing with ethanol (EtOH) for three times, and finally, kept in EtOH until time of use. The molar ratio of (P + B)/Ni was 8/1 to ensure the complete reduction of Ni^{2+} ions. The P- and B-contents in the Ni–P–B samples were adjusted by varying the molar ratio of P/B. For comparison, Ni–P and Ni–B samples were also prepared in the similar ways by using either NaH_2PO_2 or KBH_4 as single reducing agent.

2.2. Catalyst characterization

The bulk composition was analyzed by means of inductively coupled plasma–atomic emission spectroscopy (ICP–AES; Jarrell-Ash Scan 2000). The amorphous structure and the crystallization process were characterized by both X-ray diffraction (XRD; Rigaku Dmax-3C) and selected area electron diffraction (SAED; JEOL JEM2011). The morphology and particle size were observed by transmission electron microscopy (TEM; JEOL JEM2011). Surface electronic state and surface composition were analyzed by X-ray photoelectron spectroscopy (XPS; PerkinElmer PHI 5000C ESCA, Mg Kα) during which the samples were dried *in situ* in pure Ar atmosphere to avoid oxidation. All the binding energy values were calibrated by using C 1s = 284.6 eV as a reference. The active surface area (S_{Ni}) was measured by hydrogen chemisorption on a Quantachrome CHEMBET 3000 instrument assuming H/Ni(s) = 1 and a surface area of 6.5×10^{-20} m^2 per Ni atom [29]. The hydrogen temperature-programmed desorption (H_2-TPD) curve was obtained on the same instrument in Ar flow at a ramping rate of 20 K/min.

2.3. Activity test

Liquid-phase hydrogenation of *p*-CNB was performed at 1.0 MPa H_2 pressure and 353 K in a 200-ml stainless steel autoclave with a Teflon tube to avoid metal contamination. Briefly, a catalyst containing 0.5 g Ni, 20 mmol of *p*-CNB, 0.8 g of *n*-$C_{12}H_{25}OH$ (as GC internal standard) and 60 ml of EtOH were mixed in the autoclave. In order to ascertain the role of mass transfer, the catalyst amount was varied from 0.1 to 1.0 g and the speed of agitation was varied from 400 to 1200 rpm. In view of the observation that there was a plateau in the dependency of the initial rate upon the stirring rate above 800 rpm and that the initial rate varied linearly with catalyst amount, it could be concluded that the stirring rate of 1000 rpm was high enough so that the hydrogenation rates were independent of mass transfer. The initial rate of reaction was obtained by measuring the drop of P_{H_2} within reaction time, from which both the specific activity (i.e., H_2 uptake rate per gram of nickel; R_H^m = mmol h^{-1} g_{Ni}^{-1}) and the areal activity (i.e., H_2 uptake rate per m^2 of the active surface area; R_H^S = mmol h^{-1} m_{Ni}^{-2}) were calculated by using the ideal gas equation. The R_H^S could be considered as the intrinsic activity since the dispersing effect of Ni active sites was excluded. During reaction, samples were withdrawn from the reaction mixture at intervals to determine the conversion and the selectivity by gas chromatograph analysis (GC 9800) equipped with a flame ionization detector (FID) under following conditions: AC-5 column, injector temperature 513 K, oven temperature programmed from 373 to 513 K at a ramping rate of 15 K/min, and carrier gas N_2, 30 ml/min. Reproducibility was checked by repeating the runs at least three times and was found to be within acceptable limits (±5%).

3. Results and discussion

SAED images of the fresh Ni–P–B, Ni–B and Ni–B samples displayed a series of diffuse Debye rings indicative of the typical amorphous structure [30], which were further confirmed by XRD patterns (Fig. 1) since only one broad peak around $2\theta = 45^\circ$ was observed [22]. The decrease in XRD peak width demonstrated that amorphous degree decreased in the order of Ni–P–B > Ni–B > Ni–P. The higher amorphous degree of Ni–B than Ni–P could be attributed to the much bigger atomic size difference between Ni (0.124 nm) and B (0.082 nm) than that between Ni and P (0.106 nm) [31]. In addition, the stronger interaction between the metallic Ni and the alloying B than that between the metallic Ni and the alloying P could also account for its higher amorphous degree [32–34]. Ni–P–B exhibited higher amorphous degree than either Ni–B or Ni–P, possibly due to self-structural disturbance by two metalloids. After being treated at temperature at 873 K for 2 h in N_2 flow, various crystalline diffraction peaks corresponding to metallic Ni and crystallized Ni–B, Ni–P and Ni–P–B appeared, indicating that these amorphous alloys were thermodynamically metastable which might undergo crystallization process, together with the decomposition of Ni–B, Ni–P and Ni–P–B alloys.

As shown in Fig. 2, the TEM and the HRTEM images revealed that the fresh Ni–B sample was present in the form of shapeless particle with a wide size distribution from 10 to 30 nm, obviously due to the agglomeration. In contrast, Ni–P sample displayed

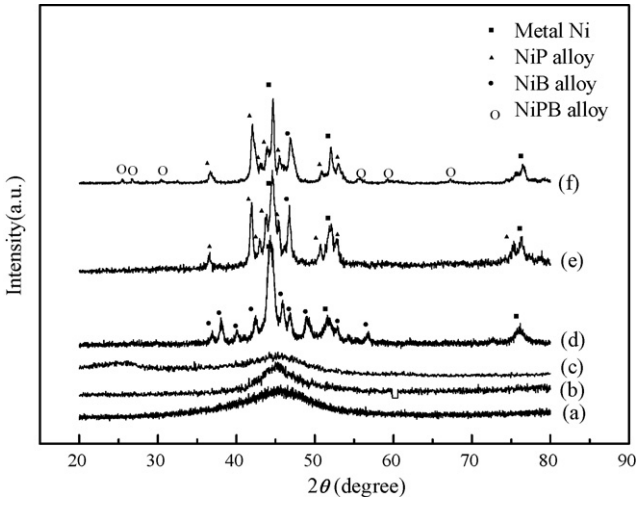

Fig. 1. XRD patterns of (a) the fresh Ni–B, (b) the fresh Ni–P, (c) the fresh Ni–P–B-3, (d) the Ni–B treated at 873 K, (e) the Ni–P treated at 873 K, and (f) the Ni–P–B-3 treated at 873 K in N_2 flow for 2 h.

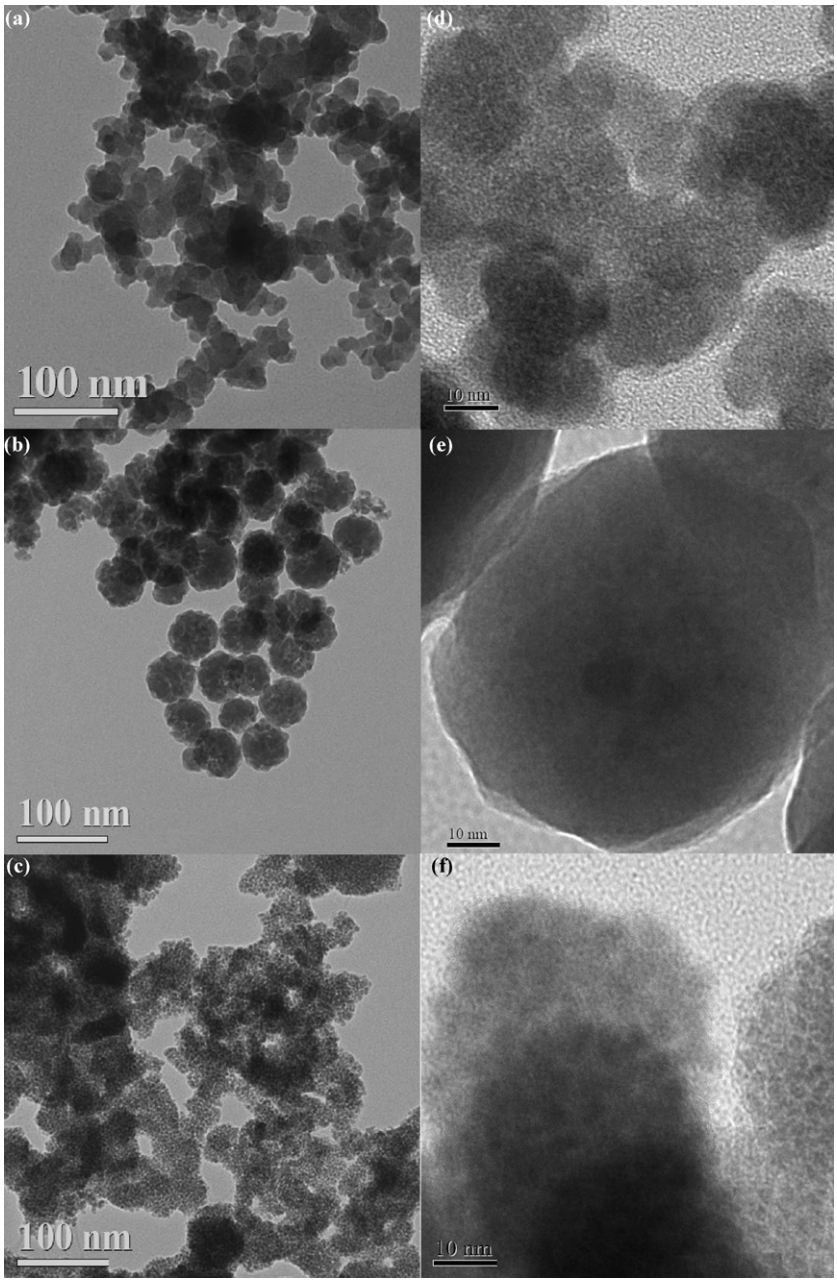

Fig. 2. TEM images of (a) the fresh Ni–B, (b) the fresh Ni–P, (c) the fresh Ni–P–B-3, and HRTEM images of (d) the fresh Ni–B, (e) the fresh Ni–P, (f) the fresh Ni–P–B-3.

regular spherical particles with the average size around 70 nm. This could be explained by considering the weaker reducibility of NaH_2PO_2 than that of KBH_4. Thus, the reduction of Ni^{2+} by NaH_2PO_2 proceeded smoothly in comparison with that by KBH_4, which might ensure the nucleation and growth of the regularly shaped particles. Ni–P–B exhibited irregular spherical particles with the average size ranged from 30 to 70 nm owing to the co-reduction of Ni^{2+} by both NaH_2PO_2 and KBH_4.

The XPS spectra (Fig. 3) revealed that nearly all the nickel species were present in metallic state corresponding to the binding energy (BE) around 853.1 eV. However, the phosphorus species in Ni–P and Ni–P–B samples were present in both oxidized state and elemental state alloying with metal Ni, corresponding to BE of 133.5 and 130.0 eV, respectively. Similarly, the boron species in Ni–B and Ni–P–B samples were also present in both oxidized state and elemental state alloying with Ni, corresponding to BE of 192.3 and 188.2 eV, respectively. In comparison with the standard BE values of pure metallic Ni, red phosphorus and amorphous boron powder, only the elemental B exhibited positive shift (ca. 1.1 eV), while no significant BE shift of the alloying P was observed in all the as-prepared samples. These observations implied that the elemental B donated partial electrons to the metal Ni in both Ni–B and Ni–P–B alloys, while no significant electron transfer between the metallic Ni and the alloying P occurred in either Ni–P or Ni–P–B, which was in good accordance with our previous results [25,35–37]. The fail-

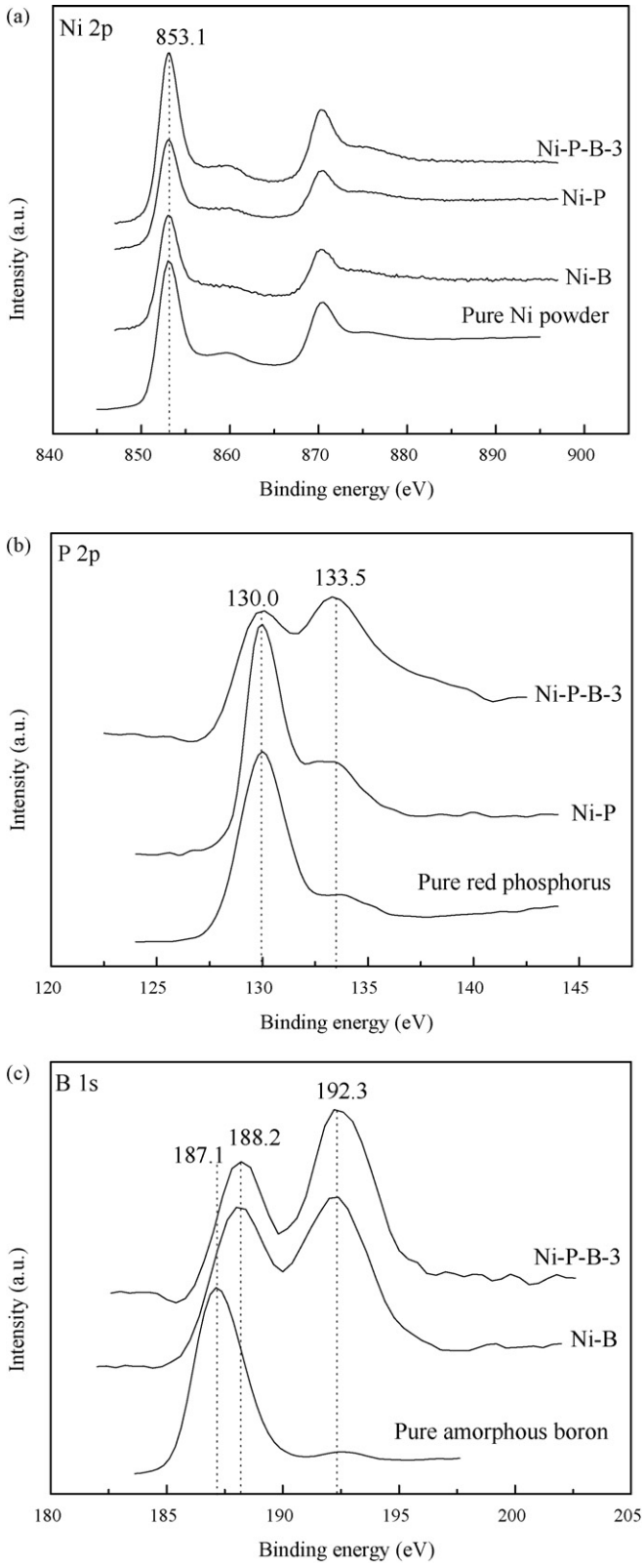

Fig. 3. XPS spectra of the as-prepared catalysts and the relative substances. (a) Ni 2p, (b) P 2p and (c) B 1s.

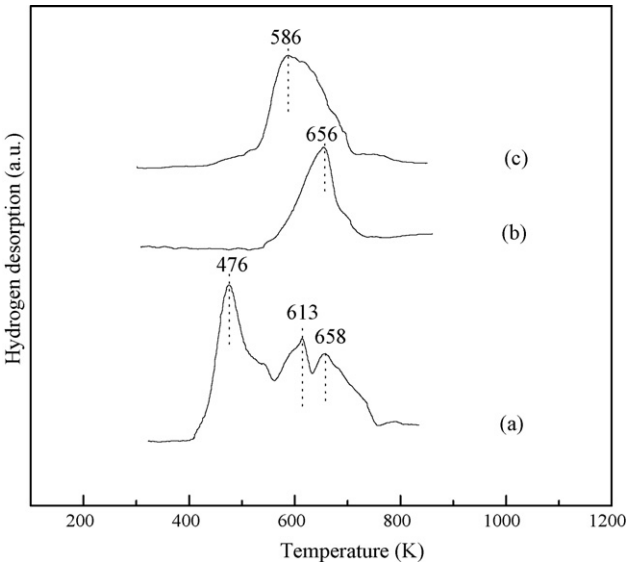

Fig. 4. H_2-TPD profiles of the as-prepared (a) Ni–B, (b) Ni–P and (c) Ni–P–B-3 catalysts. The profiles are normalized for the amount of sample used.

ure in observing the change of BE of the metallic Ni could be attributed to its bigger atomic size relative to B atom.

Fig. 4 showed the H_2-TPD curves of Ni–B, Ni–P and Ni–P–B samples. Ni–P exhibited only one TPD peak around 656 K, implying that Ni–P contained relatively uniform active sites, possibly owing to the uniform particle size and the homogeneous composition (Ni_3P). Ni–B exhibited three TPD peaks around 476, 613 and 658 K, indicating the presence of three kinds of active sites for hydrogen adsorption, possibly corresponding to the Ni_2B, Ni_3B, and Ni_4B species [38]. Besides the difference in the number of TPD peaks, it was also found the principal TPD peak in Ni–B located at much lower temperature (~476 K) than that in Ni–P (656 K), indicating that Ni–P adsorbed hydrogen more strongly than Ni–B. Two possible explanations exist to account for this difference in strength of hydrogen adsorption. EXAFS analysis revealed that the metallic Ni in Ni–P was more highly unsaturated [32,39], which might strengthen the adsorption bonding for hydrogen. On the other hand, according to the aforementioned XPS analysis, partial electrons transferred from B to metallic Ni in Ni–B amorphous alloy while no significant electron transfer occurred in Ni–P. Generally speaking, hydrogen desorption from the electron-enriched Ni active sites was easier [40]. Ni–P–B exhibited only one broad peak around 586 K, showing the synergistic effects of both P and B alloying with the metallic Ni since the mechanical mixture of Ni–B and Ni–P displayed four TPD peaks within 476–656 K corresponding to Ni–B and Ni–P.

Other structural parameters are summarized in Table 1. By calculating the peak areas of elemental nickel, phosphorus and boron, the surface compositions of Ni–B, Ni–P, and all Ni–P–B catalysts are determined [35,36]. Obviously, all catalysts had similar surface Ni content and the P/B molar ratio in Ni–P–B could be regulated freely. Ni–B exhibited much higher S_{Ni} than Ni–P owing to the smaller particle size (see TEM morphologies), which could also account for the medium S_{Ni} value of Ni–P–B in comparison with those of Ni–B and Ni–P.

Table 1
Structural properties and catalytic performances of the as-prepared catalysts[a]

Catalyst	Composition (atom%)	Surface composition (atom%)	S_{Ni} (m^2/g)	R_H^m(mmol h^{-1} g_{Ni}^{-1})	R_H^S(mmol h^{-1} m_{Ni}^{-2})	Yield (%)[b]
Ni–B	$Ni_{68.6}B_{31.4}$	$Ni_{89.3}B_{10.7}$	12.0	57.2	4.8	69.3
Ni–P	$Ni_{81.0}P_{19.0}$	$Ni_{89.8}P_{10.2}$	4.6	43.9	9.6	84.3
Ni–P–B-1	$Ni_{73.9}P_{11.0}B_{15.1}$	$Ni_{89.6}P_{4.0}B_{6.4}$	6.1	87.6	14.4	90.2
Ni–P–B-2	$Ni_{73.1}P_{15.9}B_{11.0}$	$Ni_{89.7}P_{5.4}B_{4.9}$	6.8	114.3	16.8	91.1
Ni–P–B-3	$Ni_{72.5}P_{19.6}B_{7.9}$	$Ni_{90.0}P_{6.6}B_{3.4}$	7.2	123.0	17.2	93.2
Ni–P–B-4	$Ni_{72.9}P_{21.5}B_{5.6}$	$Ni_{89.5}P_{8.1}B_{2.4}$	5.8	74.8	12.9	88.4

[a] Reaction conditions: 20 mmol of *p*-CNB; 60 ml of EtOH; each catalyst contained 0.50 g Ni; $T = 353$ K; $P_{H_2} = 1.0$MPa; stirring rate = 1000 rpm.
[b] The maximum yield of *p*-CAN.

Table 1 revealed that the ternary Ni–P–B catalysts exhibited much higher initial activity (R_H^m) and maximum *p*-CAN yield than either Ni–B or Ni–P. This must be due to the synergistic promotions from both the alloying P and the alloying B on the catalytic performances of the Ni active sites (as elucidated by the subsequent discussion). Meanwhile, it can be clearly seen that the activity was dependent on the P/B molar ratio in Ni–P–B catalysts and R_H^m of Ni–P–B first increased and then decreased with further increasing the P/B ratio. The maximum R_H^m(123.0mmol h^{-1} g_{Ni}^{-1}) was obtained on Ni–P–B-3.

Table 1 also revealed that R_H^m changed in the order of Ni–P–B > Ni–B > Ni–P, while R_H^S changed in the order of Ni–P–B > Ni–P > Ni–B. The higher R_H^S value of Ni–P than Ni–B indicated its higher intrinsic activity. The kinetic studies (see Fig. 5) revealed that *p*-CNB hydrogenation was first-order with respect to hydrogen and zero-order to *p*-CNB. Thus, the higher intrinsic activity of Ni–P relative to Ni–B could be mainly attributed to the stronger hydrogen adsorption (as confirmed by aforementioned H_2-TPD), which could enhance the surface concentration of the adsorbed hydrogen during the competitive adsorption against *p*-CNB, leading to the enhanced intrinsic activity. Despite the lower R_H^S, Ni–B amorphous alloy still exhibited higher R_H^m than Ni–P, obviously owing to the higher dispersion of Ni active sites (see S_{Ni} values). Ni–P–B catalyst exhibited much higher R_H^m owing to the synergistic promoting effects of the alloying B and the alloying P in which B enhanced the dispersion degree of Ni active sites while P enhanced the intrinsic activity. The mechanically mixed Ni–B and Ni–P showed much lower R_H^S(6.0mmol h^{-1} g_{Ni}^{-1}) and R_H^m(49.7mmol h^{-1} m_{Ni}^{-2}) than Ni–P–B, obviously due to the absence of synergistic promoting effects.

The dependency of *p*-CAN selectivity on *p*-CNB conversion during *p*-CNB hydrogenation (attached in Fig. 6c) reveals that

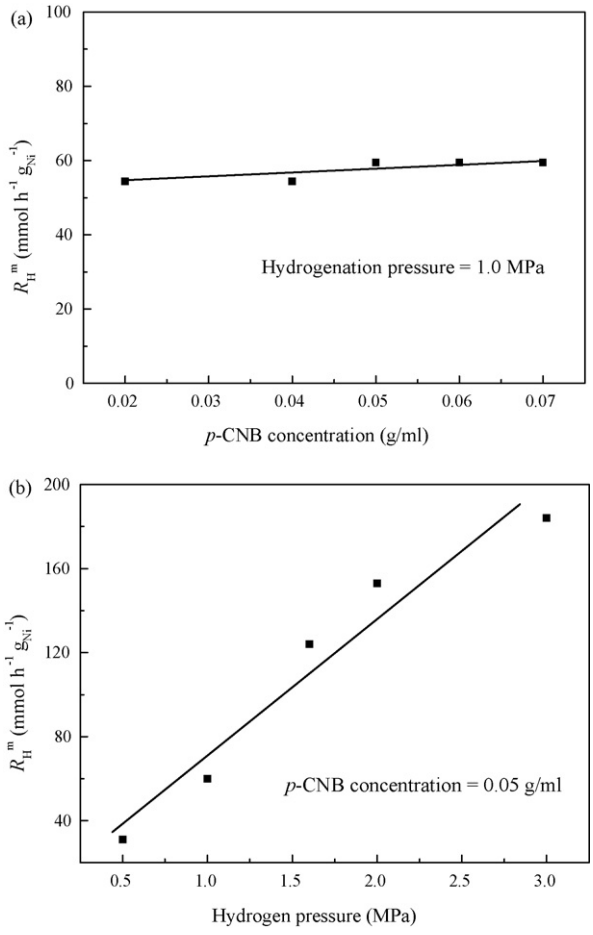

Fig. 5. Effects of (a) *p*-CNB concentration and (b) hydrogen pressure on the R_H^m over Ni–P–B-3 amorphous alloy catalyst. Reaction conditions: catalyst containing 0.5 g Ni, 60 ml of EtOH, $T = 353$ K, stirring rate = 1000 rpm. (a) $P_{H2} = 1.0$ MPa, (b) 20 mmol of *p*-CNB.

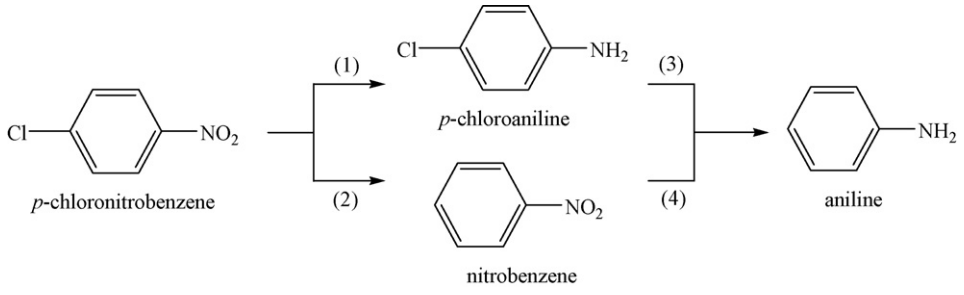

Scheme 1. A plausible mechanism of *p*-CNB hydrogenation.

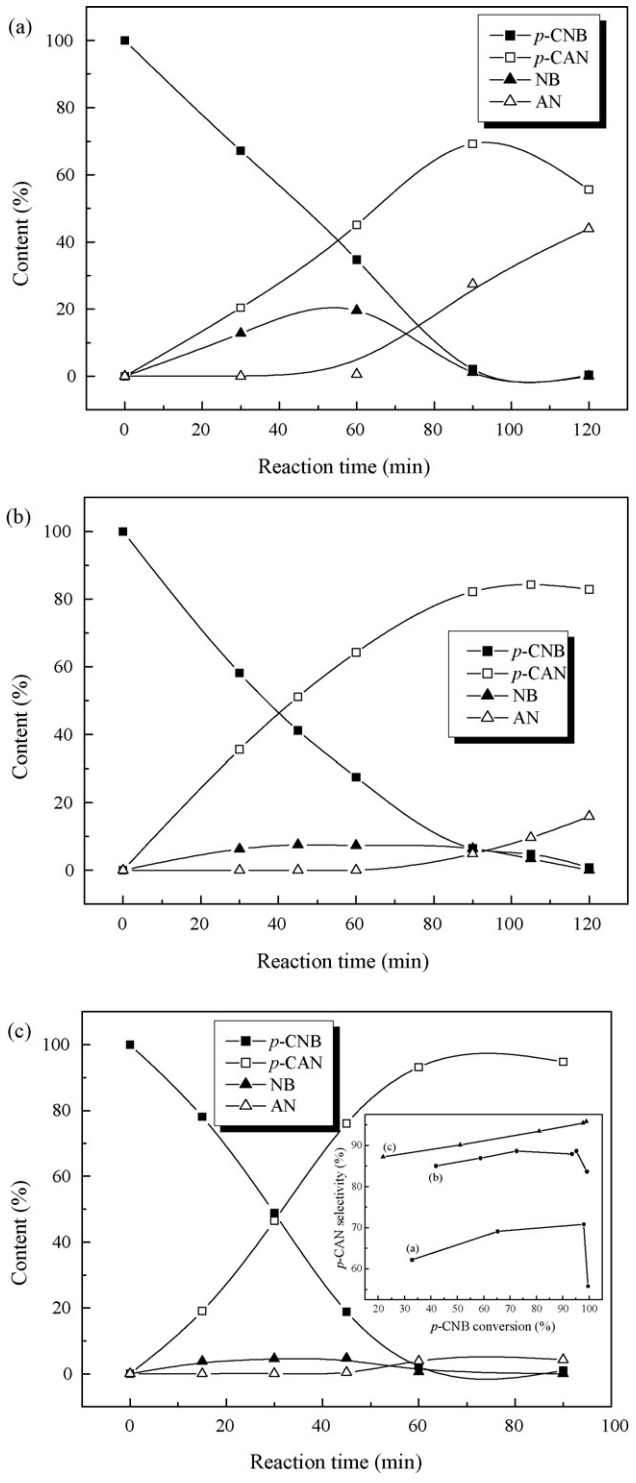

Fig. 6. Reaction profiles of *p*-CNB hydrogenation over (a) Ni–B, (b) Ni–P and (c) Ni–P–B-3 amorphous alloy catalysts. The insert is the dependency of selectivity to *p*-CAN on *p*-CNB conversion during *p*-CNB hydrogenation over (a) Ni–B, (b) Ni–P and (c) Ni–P–B-3 amorphous alloy catalysts. Reaction conditions: catalyst, 0.5 g Ni; *p*-CNB, 20 mmol; ethanol, 60 ml; *T*, 353 K; P_{H_2}, 1.0 MPa; stirring rate, 1000 rpm.

the selectivity changed in the trend of Ni–P–B > Ni–P > Ni–B, which was in accordance with the change of *p*-CAN yield (see Table 1). The synergistic promoting effects could also account for the higher selectivity obtained on Ni–P–B amorphous catalyst. According to the reaction pathway (Scheme 1), besides the main product (*p*-CAN), two side products could be formed during *p*-CNB hydrogenation. Nitrobenzene (NB) resulted from *p*-CNB hydrodehalogenation while aniline (AN) resulted from the further hydrogenation of NB and/or hydrodehalogenation of *p*-CAN. As shown in Fig. 6, Ni–P amorphous catalyst was more selective to *p*-CAN than Ni–B owing to the inhibition on the hydrodehalogenation of *p*-CNB, corresponding to the less content of NB. Ni–P–B exhibited the highest selectivity to *p*-CAN due to the effective inhibition on the hydrodehalogenations of both *p*-CNB and *p*-CAN, taking into account that the yield of *p*-CAN obtained on either Ni–P or Ni–B might decrease if the reaction time was too long while the *p*-CAN yield on Ni–P–B might remain at the maximum value (see Fig. 6). According to the adsorption mechanism, the Ni active sites might adsorb *p*-CNB via either nitro group or chlorine atom. The former was favorable for the hydrogenation of nitro group to form *p*-CAN while the latter favored the hydrodehalogenation, resulting in the formation of byproducts. *p*-CNB was a conjugated system containing nitro group, chlorine atom, and benzene ring in which partial electrons transferred from chlorine to nitro group owing to the higher electronegativity of both nitrogen and oxygen atoms than chlorine, making nitro group electron-enriched while chlorine electron-deficient. The aforementioned XPS spectra demonstrated that the metallic Ni in Ni–B was electron-enriched while no significant electron transfer occurred in Ni–P sample. The relatively less electron density on the metallic Ni in either Ni–P or Ni–P–B made it easy to adsorb electron-enriched nitro group in *p*-CNB molecule, corresponding to higher selectivity to *p*-CAN than that obtained on Ni–B. Meanwhile, according to the H_2-TPD curves, Ni–B contained at least three kinds of active sites while both Ni–P and Ni–P–B contained only one kind of active sites, corresponding to higher selectivity. In addition, both Ni–P and Ni–P–B exhibited stronger adsorption for hydrogen than Ni–B, which was favorable for the selectivity to *p*-CAN since the hydrogenation of nitro group usually needed strongly adsorbed hydrogen atoms. Furthermore, the relatively larger particle size and regular particle shape resulted from the formation of Ni–P and Ni–P–B alloys might also facilitate the adsorption of nitro group existed in the conjugated system with benzene ring and thus was favorable for the selectivity to *p*-CAN [41]. The higher selectivity to *p*-CAN on Ni–P–B than that on Ni–P could be attributed to the synergistic effects of both the alloying P and the alloying B. On the one hand, the presence of alloying P ensured the preferential adsorption of nitro group on the Ni active sites against the adsorption of chlorine atom in *p*-CNB molecule. On the other hand, the presence of alloying B could further strengthen the adsorption for nitro group via a side-bonding since the alloying B was also electron-deficient [42], which could be supported by the relatively higher selectivity to *p*-CAN over Ni–B (70.8%) than that over Raney Ni (60.9% at *p*-CNB conversion of 93.7% corresponding to the maximum *p*-CAN yield). In addition, the alloying B might also adsorb amine group (NH_2) resulted from the hydrogenation of nitro group, which could inhibit the poisoning effect of the amine group on the metallic Ni active sites, and thus promote *p*-CNB hydrogenation [27].

4. Conclusions

The above results show that, Ni–P–B amorphous alloy catalyst exhibited higher activity and better selectivity to *p*-CAN in liquid-phase *p*-CNB hydrogenation than either Ni–P or Ni–B amorphous alloy catalysts, obviously owing to the synergistic effects of both the alloying P and the alloying B. On the one hand, the presence of the alloying P could strengthen hydrogen adsorption on the Ni active site owing to the more highly unsaturated coordination, which could account for its higher intrinsic activity (R_H^S). The co-presence of the alloying B could enhance the dispersion degree of the Ni active sites owing to the stronger interaction between the metal Ni and the alloying B and thus, could enhance the apparent activity (R_H^m). On the other hand, the alloying between the P and the metallic Ni led to stronger adsorption for hydrogen and the formation of uniform particles with relatively larger size, which was favorable for the hydrogenation of nitro group to produce *p*-CAN. Meanwhile, the relatively less electron density on the metallic Ni caused by alloying P might be favorable for the competitive adsorption of nitro group against that of chlorine atom in *p*-CNB, which could effectively inhibit the hydrodehalogenation to produce side products. The co-presence of the alloying B could further enhance the adsorption of nitro group via a side-bonding and inhibit the amine poisoning on Ni active sites via adsorption the amine group resulted from *p*-CNB hydrogenation, which also promoted the selectivity to *p*-CAN.

Acknowledgements

This work was supported by the 973 Program (2005CCA01100), the 863 Project (2007AA03Z339), the National Natural Science Foundation of China (20603023), and the Shanghai Government (05QMX1442, 0552nm036, T0402, 05DZ20, 06JC14093).

References

[1] A.J. Béchamp, Anal. Chim. Phys. 42 (1854) 18.
[2] E. Thomas, J. Nickson, J. Org. Chem. 51 (1986) 3903.
[3] W.F. Hoelderich, Catal. Today 62 (2000) 115.
[4] B. Chen, U. Dingerdissen, J.G.E. Krauter, H.G.J.L. Rotgerink, K. Möbus, D.J. Ostgard, P. Panster, T.H. Riermeier, S. Seebald, T. Tacke, H. Trauthwein, Appl. Catal. A: Gen. 280 (2005) 17.
[5] C.F. Winans, J. Am. Chem. Soc. 61 (1939) 3564.
[6] R. Baltzly, A.P. Phillips, J. Am. Chem. Soc. 68 (1946) 261.
[7] W.P. Dunworth, F.F. Nord, J. Am. Chem. Soc. 74 (1952) 1459.
[8] H. Greenfield, F.S. Dovell, J. Org. Chem. 32 (1967) 3670.
[9] B. Coq, A. Tijani, F. Figuéras, J. Mol. Catal. 68 (1991) 331.
[10] B. Coq, A. Tijani, F. Figuéras, J. Mol. Catal. 71 (1992) 317.
[11] B. Coq, A. Tijani, R. Dutartre, F. Figuéras, J. Mol. Catal. A: Chem. 79 (1993) 253.
[12] P.N. Rylander, in: J.R. Anderson, M. Boudart (Eds.), Catalysis-Science and Technology, vol. 4, Akademie–Verlag, Berlin, 1993, p. 1.
[13] V.R. Chandrashekhar, R.V. Chaudhari, Ind. Eng. Chem. Res. 33 (1994) 1645.
[14] H. Arnold, F. Döbert, J. Gaube, in: G. Ertl, H. Knözinger, J. Weitkamp (Eds.), Handbook of Heterogeneous Catalysis, vol. 5, VCH, Weinheim, 1997, p. 2165.
[15] K. Wessermel, H.J. Arpe, Industrial Organic Chemistry, 3rd ed., VCH, Weinheim, 1997.
[16] B. Coq, F. Figuéras, Coord. Chem. Rev. 178–180 (1998) 1753.
[17] T. Mallar, A. Baiker, Appl. Catal. A: Gen. 200 (2000) 3.
[18] V. Kratky, M. Kralik, M. Mecarova, M. Stolcova, L. Zalibera, M. Hronec, Appl. Catal. A: Gen. 235 (2002) 225.
[19] X. Han, R. Zhou, X. Zheng, H. Jiang, J. Mol. Catal. A: Chem. 193 (2003) 103.
[20] X.X. Han, R.X. Zhou, G.H. Lai, B.H. Yue, X.M. Zheng, Catal. Lett. 89 (2003) 255.
[21] X.X. Han, R.X. Zhou, G.H. Lai, X.M. Zheng, Catal. Today 93–95 (2004) 433.
[22] J.V. Wonterghem, S. Mørups, C.J.W. Koch, S.W. Charles, S. Wells, Nature 322 (1986) 622.
[23] A. Molnar, G.V. Smith, M. Bartok, Adv. Catal. 36 (1989) 329.
[24] Y. Chen, Catal. Today 44 (1998) 3.
[25] J.F. Deng, H.X. Li, W.J. Wang, Catal. Today 51 (1999) 113.
[26] M.H. Wang, H.X. Li, Chin. J. Catal. 22 (2001) 287.
[27] X.H. Yan, J.Q. Sun, Y.W. Wang, J.F. Yang, J. Mol. Catal. A: Chem. 252 (2006) 17.
[28] W.J. Wang, J.H. Shen, Y.W. Chen, Ind. Eng. Chem. Res. 45 (2006) 8860.
[29] J.J.F. Scholten, A.P. Pijers, A.M.L. Hustings, Catal. Rev.-Sci. Eng. 27 (1985) 151.
[30] T. Osaka, K. Arai, N. Masubuchi, Y. Yamazaki, T. Namikawa, Jpn. J. Appl. Phys. 28 (1989) 866.
[31] O.N. Senkov, D.B. Miracle, Mater. Res. Bull. 36 (2001) 2183.
[32] R.P. Messmer, Phys. Rev. B 23 (1981) 1616.
[33] C. Hausleitner, J. Hafner, Phys. Rev. B 47 (1993) 5689.
[34] Z.G. Fang, B.R. Shen, J. Lu, K.N. Fan, J.F. Deng, Acta Chim. Sinica 57 (1999) 894.
[35] J.F. Deng, J. Yang, S.S. Sheng, H.R. Chen, G.X. Xiong, J. Catal. 150 (1994) 434.
[36] H. Li, H.X. Li, W.L. Dai, W.J. Wang, Z.G. Fang, J.F. Deng, Appl. Surf. Sci. 152 (1999) 25.
[37] S.Q. Wei, X.G. Wang, S.L. Yin, C.R. Chen, W.H. Liu, X.Y. Zhang, Chin. J. Catal. 22 (2001) 113.
[38] B. Shen, S. Wei, K. Fan, J.F. Deng, Appl. Phys. A 65 (1997) 295.
[39] G.D. Angel, J.L. Benitez, J. Mol. Catal. 94 (1994) 409.
[40] S. Yoshida, H. Yamashita, T. Funabiki, T. Yonezawa, J. Chem. Soc., Faraday Trans. 1 (80) (1984) 1435.
[41] B. Coq, F. Figueras, Coord. Chem. Rev. 178–180 (1998) 1753.
[42] X. Han, R. Zhou, G. Lai, X. Zheng, Catal. Today 93–95 (2004) 433.